On the Benefit of Long-Horizon Direct Model Predictive Control for Drives with LC Filters

Tobias Geyer, *Senior Member, IEEE*, Petros Karamanakos, *Member, IEEE*, and Ralph Kennel, *Senior Member, IEEE*

***Abstract*—Even though direct model predictive control (MPC) schemes almost exclusively use a prediction horizon of one in power electronics applications, the use of longer horizons offers significant performance benefits. This statement is underlined in this paper for a medium-voltage variable speed drive system, which consists of a three-level inverter, an LC filter and an induction machine. The proposed MPC controller simultaneously regulates the inverter current, capacitor voltage and stator current along given references, by manipulating the switch positions of the inverter. As will be shown, extending the prediction horizon significantly reduces the oscillations due to the filter resonance. For sufficiently long horizons, such as ten, low total harmonic distortions of the stator current can be achieved at low device switching frequencies. An additional active damping loop is not required, adding to the conceptual simplicity of the proposed control scheme.**

I. Introduction

Since the mid 2000s, model predictive control (MPC) [1] has been receiving increased attention by the power electronics community, particularly so called *direct* MPC methods that directly manipulate the switch positions of the semiconductors and hence do not require a modulator [2], [3]. The control problem is formulated as a reference tracking problem, in which any quantity of the power electronic system, such as a current, electromagnetic torque, angular speed, flux linkage, neutral point potential, real and reactive power, etc., can be regulated along a given reference [4]. This approach is often referred to as finite control set (FCS) MPC. According to the optimal control paradigm [1], a penalty on the switching effort should be added, but is alas often omitted. The optimization problem underlying direct MPC is a linear or nonlinear mixed-integer program [5], [6], which is predominantly solved using enumeration [7].

In FCS MPC, the prediction horizon is almost always set to one [8]. Indeed, it is commonly believed that a horizon of one suffices and that the use of longer horizons carries no performance benefits. This common belief might result from the fact that due to the combinatorial explosion of the number of possible solutions, investigating the potential benefits of long horizons is intrinsically hard, and horizons of two or three often offer only an incremental benefit [9]. Another reason might be that researchers have so far mostly focused on inverters directly connected to the load, such as an RL load [7]. In an orthogonal coordinate system, the fast (current) dynamic of such a setup constitutes a first-order system, i.e. in each coordinate axis the transfer function from the manipulated variable (the inverter voltage) to the load current (the controlled variable) is of first order, implying that these power electronic systems can be controlled with ease.

For these reasons, very few results are available in the literature with prediction horizons exceeding one, despite the fact that there are a few strategies that allow the implementation of demanding MPC schemes with long prediction horizons in real time [10], [11]. With regard to direct MPC and reference tracking, i.e. FCS MPC, the authors are aware of only two exceptions, namely [12], in which a horizon of two is used, and [13]. In the latter, a heuristic is proposed to reduce the number of switching sequences for longer horizons[1]. In addition to that, an FCS MPC scheme was proposed in [14] with a one-step control horizon, but with a long output horizon of up to ten steps.

To solve the control problem for long prediction horizons such as ten, a branch and bound technique called sphere decoding can be successfully adopted [15], [16]. For a three-level converter, when increasing the prediction horizon from one to ten, the current distortions can be reduced by 20%, while keeping the switching frequency constant [9]. The main benefit of long horizons, however, is expected to become evident when considering power electronic systems of so called higher order. In an orthogonal coordinate system, the fast dynamics of such systems feature more than one state variable per coordinate axis. As an example, consider an inverter driving an induction machine via an intermediate LC filter [14], [17], [18]. Ignoring the rotor dynamics, which are slow compared to the dynamics of the stator and LC filter, this system constitutes two third-order systems in an orthogonal coordinate system. To control such systems, it is common practice to design two single-input single-output (SISO) PI controller for the inverter current and to add an additional active damping loop that reigns in the higher-order system, in this case its filter resonance [19].

Another more elegant—and in the end more promising—approach is proposed in this paper that treats the higher-order

T. Geyer is with ABB Corporate Research, 5405 Baden-Dättwil, Switzerland; e-mail: t.geyer@ieee.org

P. Karamanakos and R. Kennel are with the Institute for Electrical Drive Systems and Power Electronics, Technische Universität München, 80333 Munich, Germany; e-mails: p.karamanakos@ieee.org, kennel@ieee.org

[1]Moreover, a two-step prediction approach has been proposed in [4]. In here, in a first step, the computation delay is compensated, followed by a standard predictive controller with horizon one. Therefore, this is considered to be a horizon one approach.

978-1-4799-5776-7/14/$31.00 ©2014 IEEE

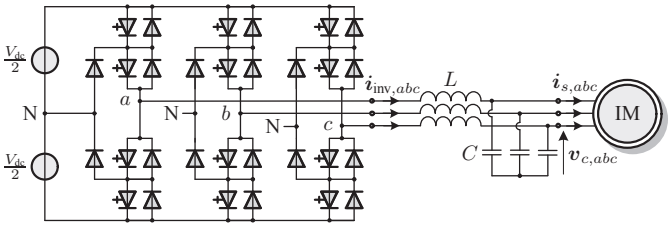

Fig. 1: (a) Three-level NPC voltage source inverter with an output LC filter driving an induction motor (IM). The inverter has a constant neutral point potential.

system as a multiple-input multiple-output (MIMO) system and designs a single MIMO controller for it. This can be easily accomplished with MPC, by regulating the inverter current, capacitor voltage and stator current simultaneously. For MPC to perform well, however, a fairly long prediction horizon is required that covers a significant fraction of the oscillation period of the filter resonance. To solve the underlying integer optimization problem, the sphere decoding algorithm is used. As an illustrative example, a neutral point clamped (NPC) inverter with a subsequent LC filter driving a medium-voltage (MV) induction machine is considered in this paper. It will be shown that for this system setup, direct MPC achieves low stator current distortions and a low device switching frequency when using a long prediction horizon. An additional damping loop is not required.

II. Physical Model of the System

Consider a variable speed drive system consisting of a three-level NPC voltage source inverter, an LC filter and a MV induction machine, as shown in Fig. 1. The dc-link voltage of the inverter V_{dc} is assumed to be constant and the neutral point potential N is fixed at zero. Note that the analysis presented below is based on normalized quantities. Moreover, as it is common practice, the transformation $\boldsymbol{\xi}_{\alpha\beta} = \boldsymbol{K}\boldsymbol{\xi}_{abc}$ is used to transform all variables $\boldsymbol{\xi}_{abc} = [\xi_a \ \xi_b \ \xi_c]^T$ from the three-phase (abc) system to $\boldsymbol{\xi}_{\alpha\beta} = [\xi_\alpha \ \xi_\beta]^T$ in the stationary and orthogonal $\alpha\beta$ system, via the transformation matrix

$$\boldsymbol{K} = \frac{2}{3}\begin{bmatrix} 1 & -\frac{1}{2} & -\frac{1}{2} \\ 0 & \frac{\sqrt{3}}{2} & -\frac{\sqrt{3}}{2} \end{bmatrix}. \tag{1}$$

Hereafter, to simplify the notation, the subscript $\alpha\beta$ is dropped from the vectors in the $\alpha\beta$ plane, unless otherwise stated.

A. Model of the Inverter

The switch positions in the three phase legs of the inverter can be represented by the integer variables $u_a, u_b, u_c \in \mathcal{U} = \{-1, 0, 1\}$. Depending on the switch position, the inverter produces the phase voltages $-\frac{V_{\text{dc}}}{2}, 0, \frac{V_{\text{dc}}}{2}$. Introducing the vector $\boldsymbol{u}_{abc} = [u_a \ u_b \ u_c]^T$, the output voltage of the inverter can be written as

$$\boldsymbol{v} = \frac{V_{\text{dc}}}{2}\boldsymbol{u} = \frac{V_{\text{dc}}}{2}\boldsymbol{K}\boldsymbol{u}_{abc}. \tag{2}$$

B. Model of the LC Filter

A symmetrical three-phase LC filter with the inductor L and its internal resistor R_1, and the capacitor C with the internal resistor R_2 is placed between the inverter and the machine to reduce the harmonic distortions at the stator windings. The state-space equations of the filter (in the $\alpha\beta$ plane) are

$$\frac{\mathrm{d}\boldsymbol{i}_{\text{inv}}}{\mathrm{d}t} = \frac{1}{L}\big(\boldsymbol{v} - R_1\boldsymbol{i}_{\text{inv}} - \boldsymbol{v}_c - R_2(\boldsymbol{i}_{\text{inv}} - \boldsymbol{i}_s)\big) \tag{3a}$$

$$\frac{\mathrm{d}\boldsymbol{v}_c}{\mathrm{d}t} = \frac{1}{C}(\boldsymbol{i}_{\text{inv}} - \boldsymbol{i}_s), \tag{3b}$$

where $\boldsymbol{i}_{\text{inv}}$ is the inverter current, $\boldsymbol{v}$ the output voltage of the inverter as given by (2), $\boldsymbol{v}_c$ the capacitor voltage and $\boldsymbol{i}_s$ the stator current. The voltage applied to the stator windings of the machine is

$$\boldsymbol{v}_s = \boldsymbol{v}_c + R_2(\boldsymbol{i}_{\text{inv}} - \boldsymbol{i}_s). \tag{4}$$

C. Model of the Machine

For the mathematical modeling of the squirrel-cage induction motor in the $\alpha\beta$ plane, the stator current $\boldsymbol{i}_s$ and the rotor flux $\boldsymbol{\psi}_r$ are chosen as state variables. The dynamic of the rotor angular speed ω_r is neglected, i.e. the speed is considered to be a time-varying parameter. The continuous-time state equations are [20]

$$\frac{\mathrm{d}\boldsymbol{i}_s}{\mathrm{d}t} = -\frac{1}{\tau_s}\boldsymbol{i}_s + \left(\frac{1}{\tau_r}\boldsymbol{I} - \omega_r\begin{bmatrix} 0 & -1 \\ 1 & 0 \end{bmatrix}\right)\frac{L_m}{\Phi}\boldsymbol{\psi}_r + \frac{L_r}{\Phi}\boldsymbol{v}_s \tag{5a}$$

$$\frac{\mathrm{d}\boldsymbol{\psi}_r}{\mathrm{d}t} = \frac{L_m}{\tau_r}\boldsymbol{i}_s - \frac{1}{\tau_r}\boldsymbol{\psi}_r + \omega_r\begin{bmatrix} 0 & -1 \\ 1 & 0 \end{bmatrix}\boldsymbol{\psi}_r. \tag{5b}$$

In (5), R_s (R_r) denotes the stator (rotor) resistance, L_{ls} (L_{lr}) the stator (rotor) reactance and L_m the mutual reactance. We also define $L_s = L_{ls} + L_m$, $L_r = L_{lr} + L_m$ and $\Phi = L_s L_r - L_m^2$. Moreover, the time-constants of the stator and rotor are $\tau_s = \frac{L_r\Phi}{R_s L_r^2 + R_r L_m^2}$ and $\tau_r = \frac{L_r}{R_r}$, respectively. $\boldsymbol{I}$ denotes the identity matrix of appropriate dimension (here two by two). All rotor quantities are referred to the stator circuit. The electromagnetic torque is given by

$$T_e = \frac{L_m}{L_r}(\boldsymbol{\psi}_r \times \boldsymbol{i}_s) = \frac{L_m}{L_r}(\psi_{r\alpha} i_{s\beta} - \psi_{r\beta} i_{s\alpha}). \tag{6}$$

III. Direct Model Predictive Control with Reference Tracking

The block diagram of the proposed MPC scheme with reference tracking is depicted in Fig. 2. The inverter switch positions are directly set by the MPC algorithm, thus not requiring the use of a modulator. The controller predicts the future evolution of the trajectories of concern as a function of the switching sequence. This prediction is based on the measurements of the inverter current, capacitor voltage and stator current, as well as on the estimate of the rotor flux, which is obtained by a flux observer. The switching sequence is chosen that minimizes a performance criterion.

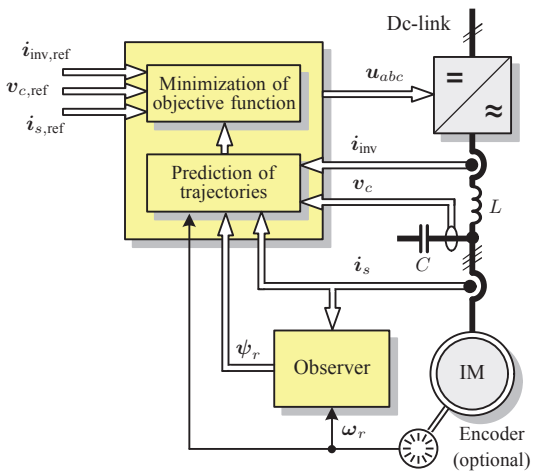

Fig. 2: Direct model predictive control with reference tracking for the drive system in Fig. 1.

A. Internal Model of the Controller

The controller is based on a discrete-time state-space model of the system, which is formulated in the $\alpha\beta$ frame. The rotor speed ω_r is assumed to be constant within the prediction horizon, which turns it into a time-varying parameter. The system state vector $\boldsymbol{x} \in \mathbb{R}^8$ includes the inverter current, capacitor voltage, stator current and rotor flux

$$\boldsymbol{x} = \begin{bmatrix} \boldsymbol{i}_{\text{inv}}^T & \boldsymbol{v}_c^T & \boldsymbol{i}_s^T & \boldsymbol{\psi}_r^T \end{bmatrix}^T . \tag{7}$$

The three-phase switch position $\boldsymbol{u}_{abc} \in \mathcal{U}^3$ constitutes the input vector, whereas the inverter current, the capacitor voltage and the stator current are the output variables, which form the output vector

$$\boldsymbol{y} = \begin{bmatrix} \boldsymbol{i}_{\text{inv}}^T & \boldsymbol{v}_c^T & \boldsymbol{i}_s^T \end{bmatrix}^T . \tag{8}$$

Based on the above and the model in Section II (see (2)–(5)), the state-space prediction model of the drive in the continuous-time domain can be derived, which is of the form

$$\frac{\mathrm{d}\boldsymbol{x}(t)}{\mathrm{d}t} = \boldsymbol{D}\boldsymbol{x}(t) + \boldsymbol{E}\boldsymbol{u}_{abc}(t) \tag{9a}$$

$$\boldsymbol{y}(t) = \boldsymbol{F}\boldsymbol{x}(t) . \tag{9b}$$

The corresponding matrices $\boldsymbol{D}$, $\boldsymbol{E}$, and $\boldsymbol{F}$ are provided in the appendix. Using exact Euler discretization, the discrete-time prediction model

$$\boldsymbol{x}(k+1) = \boldsymbol{A}\boldsymbol{x}(k) + \boldsymbol{B}\boldsymbol{u}_{abc}(k) \tag{10a}$$

$$\boldsymbol{y}(k) = \boldsymbol{C}\boldsymbol{x}(k) , \tag{10b}$$

results with $\boldsymbol{A} = \mathbf{e}^{\boldsymbol{D}T_s}$, $\boldsymbol{B} = -\boldsymbol{D}^{-1}(\boldsymbol{I} - \boldsymbol{A})\boldsymbol{E}$ and $\boldsymbol{C} = \boldsymbol{E}$.

Furthermore, $\mathbf{e}$ is the matrix exponential, T_s the sampling interval, $k \in \mathbb{N}$, and $\boldsymbol{I}$ is—as previously defined—the identity matrix.

B. Constrained Optimal Control Problem

The control objectives are the following. The stator current $\boldsymbol{i}_s$ should track its reference $\boldsymbol{i}_{s,\text{ref}}$ accurately, and the total harmonic distortion (THD) of the stator current should be small. Similarly, the inverter current $\boldsymbol{i}_{\text{inv}}$ and the capacitor voltage $\boldsymbol{v}_c$ are to follow their respective reference values. The switching frequency is to be minimized.

At time-step k, these control objectives can be mapped into the objective function

$$J(k) = \sum_{\ell=k}^{k+N-1} ||\boldsymbol{y}_{\text{ref}}(\ell+1|k) - \boldsymbol{y}(\ell+1|k)||_{\boldsymbol{Q}}^2 + ||\Delta\boldsymbol{u}_{abc}(\ell|k)||_{\boldsymbol{R}}^2 , \tag{11}$$

which penalizes the variables of interest over the finite prediction horizon of N time steps. In (11) $\boldsymbol{y}_{\text{ref}} = [\boldsymbol{i}_{\text{inv,ref}}^T \; \boldsymbol{v}_{c,\text{ref}}^T \; \boldsymbol{i}_{s,\text{ref}}^T]^T \in \mathbb{R}^6$ holds the reference values of the six output variables. The term $\Delta\boldsymbol{u}_{abc}(k) = \boldsymbol{u}_{abc}(k) - \boldsymbol{u}_{abc}(k-1)$ relates to the switching effort; by adding it to the objective function, the inverter switching frequency can be minimized. Finally, $\boldsymbol{Q}$ and $\boldsymbol{R}$ are the weighting matrices[2], where $\boldsymbol{Q} \in \mathbb{R}^{6\times6}$, and $\boldsymbol{R} \in \mathbb{R}^{3\times3}$ are diagonal and positive definite matrices.

The penalties on the deviations of the output variables from their references, $\boldsymbol{i}_{\text{inv,ref}} - \boldsymbol{i}_{\text{inv}}, \boldsymbol{v}_{c,\text{ref}} - \boldsymbol{v}_c, \boldsymbol{i}_{s,\text{ref}} - \boldsymbol{i}_s$, i.e. the diagonal entries of $\boldsymbol{Q}$, differ from each other. They allow one to prioritize the tracking accuracy among the three output variables. Typically, priority is given to the stator current, by choosing large penalties for the corresponding diagonal entries in $\boldsymbol{Q}$. The diagonal entries of $\boldsymbol{R}$ are equal, i.e. $\boldsymbol{R} = \lambda_u \boldsymbol{I}$, with $\lambda_u \in \mathbb{R}^+$. The ratio between $\boldsymbol{R}$ and $\boldsymbol{Q}$ decides on the trade-off between the overall tracking accuracy and the switching effort. When the tracking of the stator current is prioritized in $\boldsymbol{Q}$, this trade-off is equivalent to the trade-off between the stator current THD and the switching frequency of the inverter.

To obtain the control input at time-step k, the objective function (11) is minimized over the optimization variable, i.e. the switching sequence $\boldsymbol{U}(k) = [\boldsymbol{u}_{abc}^T(k) \; \boldsymbol{u}_{abc}^T(k+1) \ldots \boldsymbol{u}_{abc}^T(k+N-1)]^T$ over the horizon N. With this, the optimization problem underlying MPC can be formulated as

$$\underset{\boldsymbol{U}(k)}{\text{minimize}} \quad J(k) \tag{12a}$$

$$\text{subject to} \quad \boldsymbol{U}(k) \in \mathbb{U} \tag{12b}$$

$$||\Delta\boldsymbol{u}_{abc}(\ell)||_\infty \leq 1 , \; \forall \ell = k, \ldots, k+N-1 , \tag{12c}$$

with $\mathbb{U} = \boldsymbol{\mathcal{U}} \times \cdots \times \boldsymbol{\mathcal{U}}$ being the N-times Cartesian product of the set $\boldsymbol{\mathcal{U}}$, where $\boldsymbol{\mathcal{U}} = \mathcal{U} \times \mathcal{U} \times \mathcal{U}$ denotes the set of discrete three-phase switch positions. Furthermore, the so-called switching constraints are imposed by (12c). Thanks to those, a shoot-through in the inverter is avoided, by ruling out switching transitions that would lead to a switching transition between the upper and lower dc-link rails, i.e. from $u = 1$ to $u = -1$, and vice versa.

The optimal switching sequence $\boldsymbol{U}^*(k)$ is obtained by minimizing (12). Out of $\boldsymbol{U}^*(k)$, only the first element $\boldsymbol{u}_{abc}^*(k)$ is applied to the inverter and the remainder of $\boldsymbol{U}^*(k)$ is discarded. At the next time-step $k+1$, the optimization procedure

[2]The squared norm weighted with the positive definite matrix $\boldsymbol{W}$ is given by $||\boldsymbol{\xi}||_{\boldsymbol{W}}^2 = \boldsymbol{\xi}^T\boldsymbol{W}\boldsymbol{\xi}$.

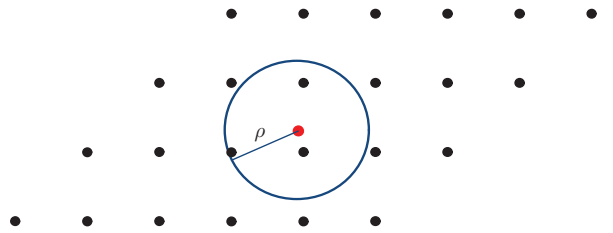

Fig. 3: The principle of the sphere decoder: A (two-dimensional) sphere of radius ρ (shown as straight (blue) line) centered at the unconstrained solution (shown as small (red) circle) includes several integer points of the lattice (shown as small (black) circles). One of these points is the integer solution of the ILS problem.

is repeated based on new measurements and estimates over a shifted prediction horizon, according to the receding horizon policy [1], which provides feedback and adds robustness to the closed-loop operation.

C. Reformulating and Solving the Optimization Problem

In a subsequent step, and in order to acquire the optimal solution $\boldsymbol{U}^*(k)$ of problem (12) in a computationally efficient manner, problem (12) is formulated as an integer least-squares (ILS) problem; by doing so the computations to be performed in real time are reduced. The procedure to rewrite the optimization problem as an ILS is similar to the one proposed in [15].

To start with, (11) can be written in vector form as

$$J = ||\boldsymbol{\Gamma x}(k) + \boldsymbol{\Upsilon U}(k) - \boldsymbol{Y}_{\text{ref}}||^2_{\boldsymbol{Q}} + ||\boldsymbol{S U}(k) - \boldsymbol{\Xi u}_{abc}(k-1)||^2_{\boldsymbol{R}}\,, \tag{13}$$

where $\boldsymbol{Y}(k)$ is the output sequence over the horizon, i.e. $\boldsymbol{Y}(k) = [\boldsymbol{y}^T(k+1)\ldots\boldsymbol{y}^T(k+N)]^T$. It is given by

$$\boldsymbol{Y}(k) = \boldsymbol{\Gamma x}(k) + \boldsymbol{\Upsilon U}(k)\,, \tag{14}$$

whereas $\boldsymbol{Y}_{\text{ref}}(k)$ is the corresponding output reference sequence, i.e. $\boldsymbol{Y}_{\text{ref}}(k) = [\boldsymbol{y}^T_{\text{ref}}(k+1)\ldots\boldsymbol{y}^T_{\text{ref}}(k+N)]^T$. The matrices $\boldsymbol{\Gamma}$, $\boldsymbol{\Upsilon}$, $\boldsymbol{S}$ and $\boldsymbol{\Xi}$ in (13) are provided in the appendix.

After performing some algebraic manipulations, (13) can be written as

$$J = (\boldsymbol{U}(k) - \boldsymbol{U}_{\text{unc}}(k))^T \boldsymbol{V} (\boldsymbol{U}(k) - \boldsymbol{U}_{\text{unc}}(k)) + \text{const}(k)\,, \tag{15}$$

where $\boldsymbol{U}_{\text{unc}} \in \mathbb{R}^n$ is the unconstrained solution to the optimization problem (12), with $n = 3N$. The positive definite matrix $\boldsymbol{V}$ is given by

$$\boldsymbol{V} = \boldsymbol{\Upsilon}^T\, \widetilde{\boldsymbol{Q}}\, \boldsymbol{\Upsilon} + \lambda_u \boldsymbol{S}^T \boldsymbol{S}\,, \tag{16}$$

where $\widetilde{\boldsymbol{Q}} = \text{diag}(\boldsymbol{Q}\ \boldsymbol{Q}\ldots\boldsymbol{Q})$.

Using the Cholesky decomposition $\boldsymbol{V}$ can be factored as

$$\boldsymbol{V}^{-1} = \boldsymbol{H}^{-1}\boldsymbol{H}^{-T}\,. \tag{17}$$

As a result, problem (12)—and after neglecting the constant term in the objective function (15)—can be rewritten as the ILS

$$\underset{\boldsymbol{U}(k)}{\text{minimize}} \quad ||\bar{\boldsymbol{U}}_{\text{unc}}(k) - \boldsymbol{H U}(k)||_2^2 \tag{18a}$$

$$\text{subject to} \quad \boldsymbol{U}(k) \in \mathbb{U} \tag{18b}$$

$$||\Delta \boldsymbol{u}_{abc}(\ell)||_\infty \leq 1\,,\ \forall\ \ell = k,\ldots,k+N-1\,, \tag{18c}$$

Algorithm 1 Sphere Decoder

```
function U* = MSphDec(U, d², i, ρ², Ū_unc)
    for each u ∈ 𝒰 do
        U_i ← u
        d'² ← ||Ū_i − H_(i,i:n) U_i:n||₂² + d²
        if d'² ≤ ρ² then
            if i < 3N then
                MSphDec(U, d'², i + 1, ρ², Ū_unc)
            else
                if U meets (18c) then
                    U* ← U
                    ρ² ← d'²
                end if
            end if
        end if
    end for
end function
```

where $\bar{\boldsymbol{U}}_{\text{unc}} \in \mathbb{R}^n$ is

$$\bar{\boldsymbol{U}}_{\text{unc}}(k) = \boldsymbol{H U}_{\text{unc}}(k)\,, \tag{19}$$

and $\boldsymbol{U} \in \mathbb{Z}^n$, $\boldsymbol{H} \in \mathbb{R}^{n\times n}$.

As shown in [15], problem (18) can be solved efficiently by adopting the notion of sphere decoding. For reasons of completeness, the sphere decoding algorithm proposed in Section V-B in [15] is briefly summarized hereafter.

The sphere decoding algorithm is a depth-first search algorithm that traverses the integer search tree in a recursive manner. When reaching the lowest level of the tree, or when pruning branches of the tree, the algorithm backtracks to explore unvisited branches in previously visited levels. For the specific problem (18), the nodes of the search tree are the elements of the switching sequences $\boldsymbol{U}$.

One can show that the optimal solution lies within an n-dimensional sphere with radius ρ that is centered at the unconstrained solution. Instead of exhaustively exploring all nodes, the sphere decoder restricts its search to this sphere, which includes only a small number of n-dimensional integer points, see Fig. 3. As a result, the computational burden is greatly reduced, since the total number of nodes, and consequently the number of switching sequences $\boldsymbol{U}$ to be explored, is in general several orders of magnitude lower than the total number of nodes in the search tree that are to be evaluated when an exhaustive search is performed, i.e. when the set of admissible sequences is fully enumerated. Note that by restricting the search to points within the sphere the optimality of the solution is not affected. Specifically, the sphere decoding algorithm obtains the same integer solution as does exhaustive enumeration.

The pseudocode of the sphere decoder is given in Algorithm 1. It should be noted that the initial values of the arguments $\boldsymbol{U}$, d^2, i, and ρ are the empty set $\emptyset$, 0, 1, and the initial radius of the sphere ρ_{init}, respectively. The latter is computed using (31) in [15].

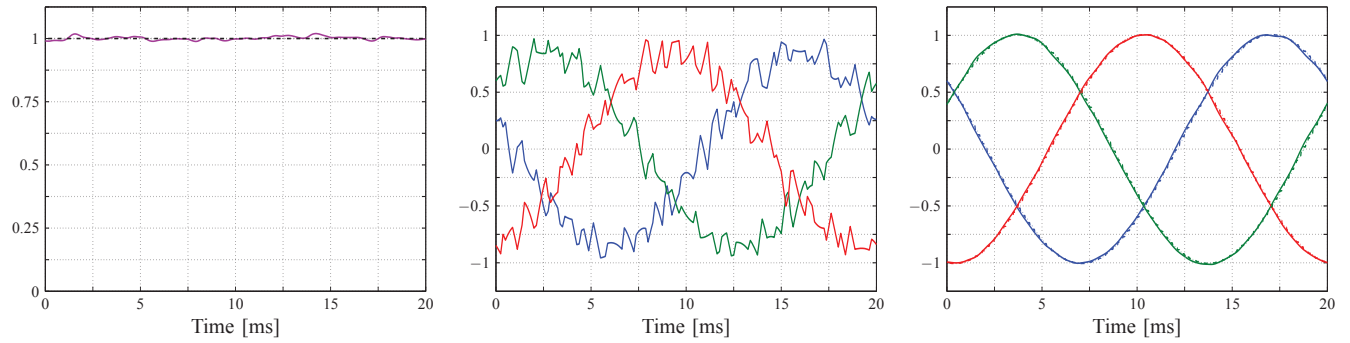

(a) Electromagnetic torque T_e (solid line) and its reference (dash-dotted line)

(b) Three-phase inverter current $\boldsymbol{i}_{\text{inv}}$

(c) Three-phase stator current $\boldsymbol{i}_s$ (solid lines) and their references (dash-dotted lines)

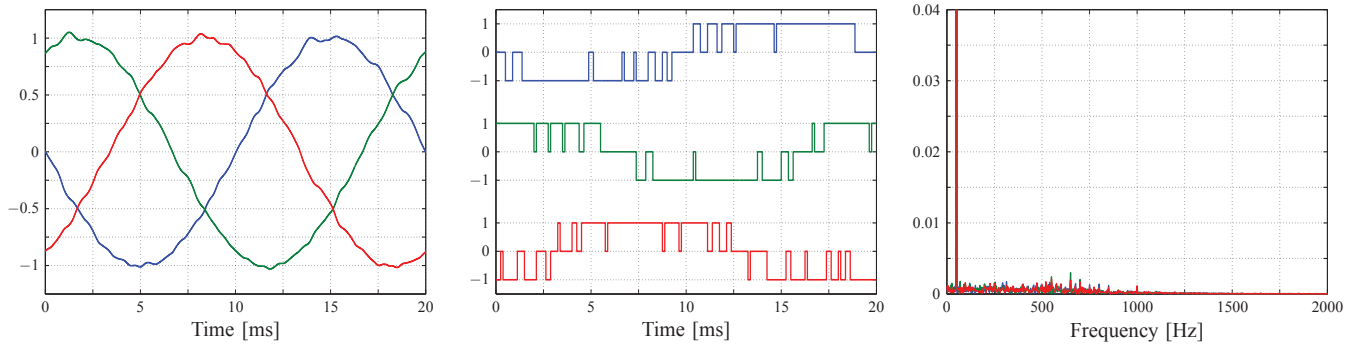

(d) Three-phase capacitor voltage v_c

(e) Switch positions $\boldsymbol{u}_{abc}$

(f) Stator current spectrum

Fig. 4: Simulated waveforms produced by the direct model predictive controller (MPC) at steady-state operation, at full speed and rated torque. The prediction horizon is set to $N = 15$ and the controller sampling interval is $T_s = 125\,\mu$s. For the device switching frequency of $f_{\text{sw}} = 303\,\text{Hz}$ the low stator current THD of $I_{s,\text{THD}} = 1.156\,\%$ is achieved.

IV. Performance Evaluation

Simulation results are presented in this section that highlight the benefits long prediction horizons entail when using direct MPC for higher-order systems. The MV drive with an LC filter as shown in Fig. 1 is used for this purpose. The NPC inverter is fed by the constant dc-link voltage of $V_{\text{dc}} = 5.2\,\text{kV}$ and a fixed neutral point potential. A 3.3 kV and 50 Hz squirrel cage induction machine rated at 2 MVA with 356 A rated current is used. The machine's total leakage inductance is $L_\sigma = 0.25\,\text{p.u.}$. The values of the LC filter are given by $L = 0.1174\,\text{p.u.}$ and $C = 2.9738\,\text{p.u.}$. The detailed parameters of the machine, inverter and LC filter are summarized in Table I. For the scenarios examined below, all results are shown in the p.u. system.

The dominant resonance of this system is constituted by the filter capacitance oscillating against the two inductances in the drive system, namely the filter inductance and the total leakage inductance of the machine. The resonance frequency is given by

$$f_{\text{res}} = \frac{1}{2\pi\sqrt{C\frac{LL_\sigma}{L+L_\sigma}}}\,. \tag{20}$$

For the given parameters, $f_{\text{res}} = 304\,\text{Hz}$ results.

The controller sampling interval $T_s = 125\,\mu$s is chosen to facilitate long prediction intervals *in time*. Even though such a relatively long sampling interval reduces the granularity of switching, it is beneficial when operating at low switching frequencies. The penalties in the objective function (11) are set to $\boldsymbol{Q} = \text{diag}(1, 1, 5, 5, 150, 150)$ and $\boldsymbol{R} = \lambda_u \boldsymbol{I}$. The weight λ_u is chosen such that the desired switching frequency is achieved.

A. Operation at Steady-State

In a first step, the performance of the long-horizon direct MPC scheme with reference tracking is investigated at steady-state conditions, when operating at nominal speed and rated torque. To ensure that the drive system has settled at steady-state operation, the system is first simulated over several fundamental periods without recording the results. The prediction horizon of $N = 15$ is investigated and $\lambda_u = 0.28$ is chosen, resulting in an average device switching frequency of $f_{\text{sw}} = 303\,\text{Hz}$, which is typical for medium-voltage applications. A very low stator current THD of $I_{s,\text{THD}} = 1.156\%$ is achieved.

The steady-state waveforms of the electromagnetic torque and three-phase inverter currents over one fundamental period are shown in Figs. 4(a) and 4(b), respectively. Throughout the paper, the phase currents in a, b, and c are shown as blue, green and red lines, respectively. Fig. 4(c) shows the three-phase stator current waveforms along with their dash-dotted references. The stator currents are effectively sinusoidal, despite operation at a low switching frequency. Fig. 4(d) displays the

TABLE I: Rated values (left) and parameters (right) of the drive system with an LC filter.

Induction motor	Voltage	3300 V	R_s	0.0108 p.u.
	Current	356 A	R_r	0.0091 p.u.
	Real power	1.587 MW	L_{ls}	0.1493 p.u.
	Apparent power	2.035 MVA	L_{lr}	0.1104 p.u.
	Frequency	50 Hz	L_m	2.3489 p.u.
	Rotational speed	596 rpm		
Inverter			V_{dc}	1.930 p.u.
LC filter			L	0.1174 p.u.
			C	2.9738 p.u.
			R_1	$3.737 \cdot 10^{-4}$ p.u.
			R_2	$3.737 \cdot 10^{-4}$ p.u.

three-phase voltage across the filter capacitors, and Fig. 4(e) depicts the three-phase switching sequence. For each phase of the stator current, the spectrum was computed using a Fourier transformation of the current waveform, which was recorded over 15 fundamental periods. The spectrum of each phase is shown separately in Fig. 4(f). To ensure a high resolution, the drive system was simulated with a sampling interval of 25 μs, despite the controller being executed and a new switch position being applied only at intervals of 125 μs.

In a second step, the influence of the prediction horizon on the THD of the stator current is investigated for a given switching frequency. Specifically, for different prediction horizons, the penalty λ_u was tuned such that effectively the same switching frequency of 300 Hz resulted. The individual simulations were approximated by a polynomial function of fifth order, as shown in Fig. 5. When using a prediction horizon of one step, a high stator current THD of 7.43% results, making the direct MPC scheme unsuitable for an industrial application. Increasing the prediction horizon slightly to three steps, however, drastically reduces the THD to 2.17%. Further increases in the prediction horizon lead to further decreases in the THD. For the prediction horizon $N = 20$ for example, a stator current THD of $I_{s,\mathrm{THD}} = 1.01\%$ is achieved when operating at the switching frequency $f_{\mathrm{sw}} = 303$ Hz.

This result is remarkable in that a very low stator current THD can be achieved with a direct MPC scheme without the addition of an outer damping loop. Note that the system has effectively no passive damping; the filter inductor and capacitor have effectively zero resistance and the stator resistance is with 0.01 p.u. very small. Moreover, it is remarkable that the optimization problem with such a long prediction horizon can be solved. Without the sphere decoder and when resorting to full enumeration, about 10^{20} switching sequences would have to be computed every 125 μs, which is computationally intractable[3].

When operating at $f_{\mathrm{sw}} = 200$ Hz, the stator current THD drops slowly from its peak of $I_{s,\mathrm{THD}} = 10.2\%$ at the prediction horizon $N = 1$ when increasing the horizon. With the horizon $N = 4$, the THD is only halved to $I_{s,\mathrm{THD}} = 5.03\%$. To half it again, the prediction horizon needs to be extended to 15 steps, resulting in $I_{s,\mathrm{THD}} = 2.43\%$. We conclude that long prediction horizons tend to be of greater benefit when operating at low device switching frequencies. This observation is in line with the results in [9].

[3]Note that the number of switching sequences is less than the theoretical upper bound of 27^{20} thanks to the switching constraint (18c).

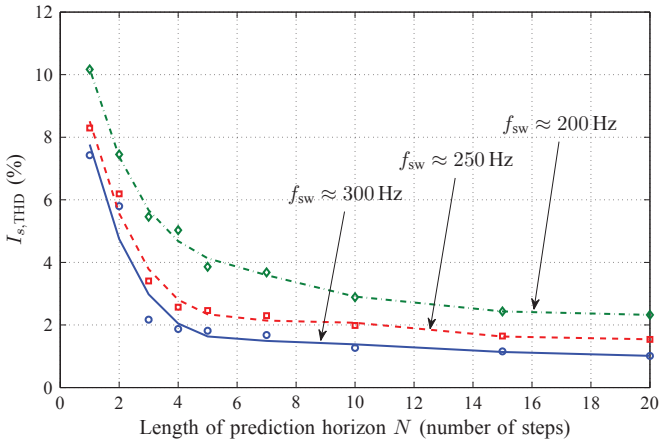

Fig. 5: Stator current THD $I_{s,\mathrm{THD}}$ as a function of the prediction horizon N for three different switching frequencies f_{sw}. The measurements are shown as (blue) circles, (red) squares, and (green) rhombi, referring to individual simulation results, when the drive was operated at switching frequencies of 300 Hz, 250 Hz and 200 Hz, respectively. The data points were approximated using fifth degree polynomials; the solid (blue) line refers to 300 Hz, the dashed (red) line to 250 Hz, and the dash-dotted (green) line corresponds to 200 Hz).

Note that the drive system can be successfully operated at switching frequencies significantly below the resonance frequency of the LC filter. For example, for the prediction horizon $N = 20$ and the penalty $\lambda_u = 9.6$, the converter operates at the switching frequency $f_{\mathrm{sw}} = 138$ Hz, which is significantly below the 304 Hz of the LC filter resonance. The resulting stator current THD is $I_{s,\mathrm{THD}} = 4.99\%$. To achieve this, the direct MPC scheme shapes the stator current spectrum, based on information extracted from the internal prediction model of the drive system, which captures the filter resonance and the effect the switching actions have on it. To successfully shape the current spectrum at low switching frequencies, long prediction horizons are required.

B. Operation during Torque Reference Steps

In a last step, the performance of the proposed direct MPC algorithm is examined during torque transients to highlight its very fast dynamical behavior. For the examined scenario, a 15-step prediction horizon is considered with the same weighting matrix $\boldsymbol{Q}$ as before. Using again the penalty $\lambda_u = 0.28$ on the switching transitions, the switching frequency $f_{\mathrm{sw}} = 300$ Hz results. While operating at rated speed, reference torque steps of magnitude one are imposed. The response of the drive system to these torque steps is shown in Fig. 6. The same subfigures as in Fig. 4 are used, except for the current spectrum, which is not shown, since it is of no relevance during transients. The torque steps on the torque reference are translated into the corresponding steady-state references $\boldsymbol{y}_{\mathrm{ref}}$ on the inverter current, capacitor voltage and stator current. The latter are shown as dash-dotted lines in Fig. 6(c).

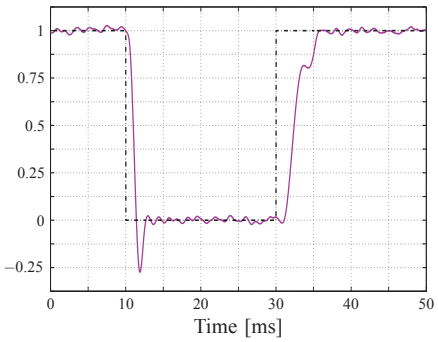

(a) Electromagnetic torque (solid line) T_e and its reference (dash-dotted line)

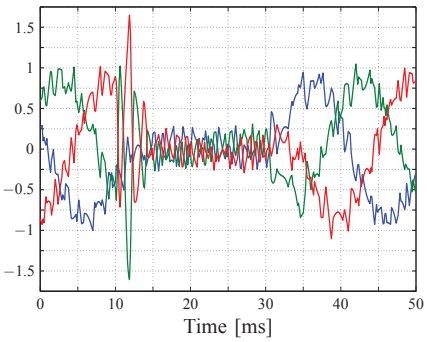

(b) Three-phase inverter current $\boldsymbol{i}_{\text{inv}}$

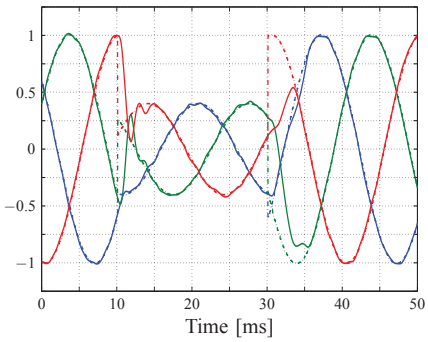

(c) Three-phase stator current $\boldsymbol{i}_s$ (solid lines) and their references (dash-dotted lines)

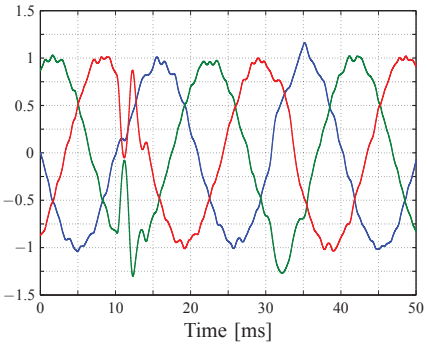

(d) Three-phase capacitor voltage v_c

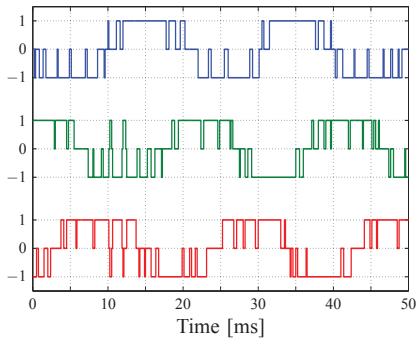

(e) Switch positions $\boldsymbol{u}_{abc}$

Fig. 6: Torque reference steps for direct MPC with the horizon $N = 15$ at nominal speed. The controller sampling interval is $T_s = 125\,\mu$s and the switching frequency is $f_{\text{sw}} = 300\,$Hz.

As can be observed in Fig. 6(e), when the torque reference is stepped down from rated torque to zero, the voltage applied to the LC filter is instantly inverted, resulting in a short torque settling time of 2.5 ms. When the torque reference is stepped up from zero to one, the transient lasts significantly longer and the steady-state operating point is reached only within 10 ms. This is due to the small voltage margin available, which is due to the machine operating at nominal speed. Nevertheless, the stator currents are quickly regulated to their new reference values, as can be seen in Fig. 6(c).

During the torque transients, significant energy is to be moved between the inverter, filter and machine. The magnitude and phase of the inverter current through the filter inductor is changed, as is the phase of the capacitor voltage, and the magnitude and phase of the machine's stator windings.

The direct MPC scheme acts effectively like a deadbeat controller. To move the third order system as quickly as possible to its new references, three notches in the switching sequence are created, which lead to three notches in the inverter current. In turn, this leads to one distinctive notch in the capacitor voltage. When voltage margin is available, i.e. when stepping the torque from one p.u. to zero, these notches can be easily identified in Fig. 6(e). When stepping the torque up, very little voltage margin is available, limiting the magnitude of the notches and the speed of the torque response.

Note the effect of the switching constraint (18c). Whenever a direct switching from -1 to 1 and vice versa is required, a mandatory intermediate zero switch position is applied for the controller sampling interval. This slightly slows down the transient performance of the controller. Nevertheless, the controller exhibits significant overshoots during the negative torque step, particularly in the inverter current. In a practical setting, this might be undesirable, necessitating the addition of a current limiting feature or the use of reference torque ramps instead of steps.

V. Conclusions

For a medium-voltage drive system with an induction machine and LC filter, a direct model predictive control (MPC) algorithm (without a modulator) was proposed with very long prediction horizons. This control method treats the drive system as a multiple-input multiple-output (MIMO) system and manipulates the inverter switch positions such that the inverter current, capacitor voltage and stator current track their respective reference in the orthogonal reference frame. The active damping of the filter resonance is achieved implicitly by the controller, making an additional active damping loop obsolete. When using long prediction horizons such as 20, low stator current THDs in the range of 1 to 2% can be achieved for device switching frequencies below the filter resonance frequency of 300 Hz.

When considering such long prediction horizons, enumeration of all possible switching sequences becomes compu-

tationally intractable. To overcome this and to solve the underlying optimization problem in real time in a computationally efficient manner, a smart branch and bound technique called sphere decoding is adopted [15]. Solving the integer least-squares (ILS) problem in this way keeps the computational complexity at bay and allows one to fully exploit the performance benefits that long prediction horizons provide. Increasing the prediction horizon from one to 20, for example, reduces the stator current THD sevenfold for the same device switching.

We conclude that in contrast to common belief, long prediction horizons do carry performance benefits for power electronic systems, particularly when considering systems of higher order or when operating them at low switching frequencies. It is straightforward to apply the proposed controller to any linear system with switched (integer) inputs, such as grid-side converters with LCL filters, making this scheme a promising alternative to the traditionally used field-oriented control methods that are based on PI current controllers and pulse width modulators.

VI. Appendix

The matrices $\boldsymbol{D}$, $\boldsymbol{E}$, and $\boldsymbol{F}$ of the continuous-time state-space model of the drive system (9) are

$$\boldsymbol{D} = \begin{bmatrix} -\frac{R_1+R_2}{L}\boldsymbol{I} & -\frac{1}{L}\boldsymbol{I} & \frac{R_2}{L}\boldsymbol{I} & \boldsymbol{0} \\ \frac{1}{C}\boldsymbol{I} & \boldsymbol{0} & -\frac{1}{C}\boldsymbol{I} & \boldsymbol{0} \\ \frac{L_r}{\Phi}R_2\boldsymbol{I} & \frac{L_r}{\Phi}\boldsymbol{I} & -(\frac{1}{\tau_s}+\frac{L_r}{\Phi}R_2)\boldsymbol{I} & p_1 \\ \boldsymbol{0} & \boldsymbol{0} & \frac{L_m}{\tau_r}\boldsymbol{I} & p_2 \end{bmatrix},$$

$$\boldsymbol{E} = \frac{V_{\mathrm{dc}}}{2}\begin{bmatrix} \frac{1}{L}\boldsymbol{I} \\ \boldsymbol{0} \\ \boldsymbol{0} \\ \boldsymbol{0} \end{bmatrix}\boldsymbol{K},\ \boldsymbol{F} = \begin{bmatrix} \boldsymbol{I} & \boldsymbol{0} & \boldsymbol{0} & \boldsymbol{0} \\ \boldsymbol{0} & \boldsymbol{I} & \boldsymbol{0} & \boldsymbol{0} \\ \boldsymbol{0} & \boldsymbol{0} & \boldsymbol{I} & \boldsymbol{0} \end{bmatrix},$$

where $\boldsymbol{0}$ is the zero matrix and $\boldsymbol{I}$ the identity matrix of appropriate dimensions. Moreover

$$p_1 = \left(\frac{1}{\tau_r}\boldsymbol{I} - \omega_r \begin{bmatrix} 0 & -1 \\ 1 & 0 \end{bmatrix}\right)\frac{L_m}{\Phi},$$

$$p_2 = \frac{1}{\tau_r}\boldsymbol{I} + \omega_r \begin{bmatrix} 0 & -1 \\ 1 & 0 \end{bmatrix}.$$

The matrices $\boldsymbol{\Upsilon}$, $\boldsymbol{\Gamma}$, $\boldsymbol{S}$, and $\boldsymbol{\Xi}$ in (13) are

$$\boldsymbol{\Upsilon} = \begin{bmatrix} \boldsymbol{CBK} & \boldsymbol{0} & \cdots & \boldsymbol{0} \\ \boldsymbol{CABK} & \boldsymbol{CBK} & \cdots & \boldsymbol{0} \\ \vdots & \vdots & & \vdots \\ \boldsymbol{CA}^{N-1}\boldsymbol{BK} & \boldsymbol{CA}^{N-2}\boldsymbol{BK} & \cdots & \boldsymbol{CBK} \end{bmatrix},$$

$$\boldsymbol{\Gamma} = \begin{bmatrix} \boldsymbol{CA} \\ \boldsymbol{CA}^2 \\ \vdots \\ \boldsymbol{CA}^N \end{bmatrix},\ \boldsymbol{S} = \begin{bmatrix} \boldsymbol{I} & \boldsymbol{0} & \cdots & \boldsymbol{0} \\ -\boldsymbol{I} & \boldsymbol{I} & \cdots & \boldsymbol{0} \\ \boldsymbol{0} & -\boldsymbol{I} & \cdots & \boldsymbol{0} \\ \vdots & \vdots & & \vdots \\ \boldsymbol{0} & \boldsymbol{0} & \cdots & \boldsymbol{I} \end{bmatrix},\ \boldsymbol{\Xi} = \begin{bmatrix} \boldsymbol{I} \\ \boldsymbol{0} \\ \boldsymbol{0} \\ \vdots \\ \boldsymbol{0} \end{bmatrix}.$$

References

[1] J. B. Rawlings and D. Q. Mayne, *Model Predictive Control: Theory and Design*. Madison, WI: Nob Hill, 2009.

[2] T. Geyer, G. Papafotiou, and M. Morari, "Model predictive control in power electronics: A hybrid systems approach," in *Proc. IEEE Conf. Decis. Control*, Seville, Spain, Dec. 2005, pp. 5606–5611.

[3] P. Cortés, M. P. Kazmierkowski, R. M. Kennel, D. E. Quevedo, and J. Rodríguez, "Predictive control in power electronics and drives," *IEEE Trans. Ind. Electron.*, vol. 55, no. 12, pp. 4312–4324, Dec. 2008.

[4] S. Kouro, P. Cortés, R. Vargas, U. Ammann, and J. Rodríguez, "Model predictive control—A simple and powerful method to control power converters," *IEEE Trans. Ind. Electron.*, vol. 56, no. 6, pp. 1826–1838, Jun. 2009.

[5] T. Geyer, "Low complexity model predictive control in power electronics and power systems," Ph.D. dissertation, Autom. Control Lab. ETH Zurich, Zurich, Switzerland, 2005.

[6] P. Karamanakos, "Model predictive control strategies for power electronics converters and ac drives," Ph.D. dissertation, Elect. Mach. and Power Electron. Lab. NTU Athens, Athens, Greece, 2013.

[7] J. Rodríguez, J. Pontt, C. A. Silva, P. Correa, P. Lezana, P. Cortés, and U. Ammann, "Predictive current control of a voltage source inverter," *IEEE Trans. Ind. Electron.*, vol. 54, no. 1, pp. 495–503, Feb. 2007.

[8] J. Rodríguez, M. P. Kazmierkowski, J. R. Espinoza, P. Zanchetta, H. Abu-Rub, H. A. Young, and C. A. Rojas, "State of the art of finite control set model predictive control in power electronics," *IEEE Trans. Ind. Informat.*, vol. 9, no. 2, pp. 1003–1016, May 2013.

[9] T. Geyer and D. E. Quevedo, "Multistep direct model predictive control for power electronics—Part 2: Analysis," in *Proc. IEEE Energy Convers. Congr. Expo.*, Denver, CO, Sep. 2013, pp. 1162–1169.

[10] T. Geyer, "Computationally efficient model predictive direct torque control," *IEEE Trans. Power Electron.*, vol. 26, no. 10, pp. 2804–2816, Oct. 2011.

[11] P. Karamanakos, T. Geyer, N. Oikonomou, F. D. Kieferndorf, and S. Manias, "Direct model predictive control: A review of strategies that achieve long prediction intervals for power electronics," *IEEE Ind. Electron. Mag.*, vol. 8, no. 1, pp. 32–43, Mar. 2014.

[12] P. Cortés, J. Rodríguez, S. Vazquez, and L. Franquelo, "Predictive control of a three-phase UPS inverter using two steps prediction horizon," in *Proc. IEEE Int. Conf. Ind. Technol.*, Viña del Mar, Chile, Mar. 2010, pp. 1283–1288.

[13] P. Stolze, P. Landsmann, R. Kennel, and T. Mouton, "Finite-set model predictive control with heuristic voltage vector preselection for higher prediction horizons," in *Proc. Eur. Power Electron. Conf.*, Birmingham, UK, Aug./Sep. 2011, pp. 1–9.

[14] T. Laczynski and A. Mertens, "Predictive stator current control for medium voltage drives with *LC* filters," *IEEE Trans. Power Electron.*, vol. 24, no. 11, pp. 2427–2435, Nov. 2009.

[15] T. Geyer and D. E. Quevedo, "Multistep direct model predictive control for power electronics—Part 1: Algorithm," in *Proc. IEEE Energy Convers. Congr. Expo.*, Denver, CO, Sep. 2013, pp. 1154–1161.

[16] P. Karamanakos, T. Geyer, and R. Kennel, "Reformulation of the long-horizon direct model predictive control problem to reduce the computational effort," in *Proc. IEEE Energy Convers. Congr. Expo.*, Pittsburgh, PA, Sep. 2014.

[17] J. K. Steinke, "Use of an *LC* filter to achieve a motor-friendly performance of the PWM voltage source inverter," *IEEE Trans. Energy Convers.*, vol. 14, no. 3, pp. 649–654, Sep. 1999.

[18] S. Mastellone, G. Papafotiou, and E. Liakos, "Model predictive direct torque control for MV drives with *LC* filters," in *Proc. Eur. Power Electron. Conf.*, Barcelona, Spain, Sep. 2009, pp. 1–10.

[19] Y. W. Li, "Control and resonance damping of voltage-source and current-source converters with *LC* filters," *IEEE Trans. Ind. Electron.*, vol. 56, no. 5, pp. 1511–1521, May 2009.

[20] J. Holtz, "The representation of ac machine dynamics by complex signal flow graphs," *IEEE Trans. Ind. Electron.*, vol. 42, no. 3, pp. 263–271, Jun. 1995.